Structural Engineering and Mechanics, *Vol. 61, No. 2 (2017) 193-207*
DOI: https://doi.org/10.12989/sem.2017.61.2.193

Nonlinear vibration analysis of an electrostatically excited micro cantilever beam coated by viscoelastic layer with the aim of finding the modified configuration

E. Poloei[a], M. Zamanian[*] and S.A.A. Hosseini[b]

Department of Mechanical Engineering, Faculty of Engineering, Kharazmi University, Mofatteh Avenue, P.O. Box 15719-14911, Tehran, Iran

(Received May 21, 2016, Revised July 30, 2016, Accepted August 9, 2016)

Abstract. In this study, the vibration of an electrostatically actuated micro cantilever beam is analyzed in which a viscoelastic layer covers a portion of the micro beam length. This proposed model is considered as the main element of mass and pollutant micro sensors. The nonlinear motion equation is extracted by means of Hamilton principle, considering nonlinear shortening effect for Euler-Bernoulli beam. The non-linear effects of electrostatic excitation, geometry and inertia have been taken into account. The viscoelastic model is assumed as Kelvin-Voigt model. The motion equation is discretized by Galerkin approach. The linear free vibration mode shapes of non-uniform micro beam i.e. the linear mode shape of the system by considering the geometric and inertia effects of viscoelastic layer, have been employed as comparison function in the process of the motion equation discretization. The discretized equation of motion is solved by the use of multiple scale method of perturbation theory and the results are compared with the results of numerical Runge-Kutta approach. The frequency response variations for different lengths and thicknesses of the viscoelastic layer have been founded. The results indicate that if a constant volume of viscoelastic layer is to be deposited on the micro beam for mass or gas sensor applications, then a modified configuration may be found by using the analysis of this paper.

Keywords: electrostatic excitation; Galerkin, micro sensor; multiple scale perturbation method; viscoelastic

1. Introduction

Microelectronic integrated circuit technology can be exploited as the mastermind of numerous systems. Micro electromechanical systems (MEMS) can expand this function by adding eye and arm in order to enable the system to sense and control the surrounding environment. To do so, the employed sensors measure different environmental phenomena such as mechanical, thermal, biological, chemical, optical and magnetic data. The gathered data is then transferred to the integrated systems to activate the actuators. Since MEMS are fabricated by micromachining technology employment, they deliver a magnificent level of performance, reliability as well as the low-cost of manufacturing process (Beeby *et al.* 2004).

Micro-cantilever or clamped micro beam is used as the principal element of many MEMS sensors. It may be used as a capacitive or resonance sensor. In micro capacitive sensors, the micro-cantilever beam is actuated by applying a DC voltage between the micro beam and an opposite fixed electrode plate. The applied DC voltage between the micro-beam and the plate deflects the movable micro-beam into the fixed electrode plate. This new position is known as static position. When the quantity under measurement such as the applied pressure on the micro beam changes, the static position changes as well. The variation of static deflection results in electricity production by the capacity alteration of the capacitor, which is composed of the movable micro-beam and the fixed electrode plate. The electric current fluctuation can be utilized to measure a multitude of quantity under measurement like pressure, mass and pollutant. In micro-resonator sensors, the combination of DC and AC voltage is used as the main source of excitation. The harmonic intrinsic attribute of AC voltage makes the micro-resonator sensors vibrate around the static deflection position. The resonance frequency variations, due to the measured quantity fluctuations, are monitored to determine the target quantity. The unfixed micro-beam becomes unstable when the voltage reaches a certain high level. Subsequently, it is magnetized towards the electrode plate. This occurrence, which is due to the nonlinear electrostatic actuation, is called 'pull-in' (Younis 2011). Concerning the micro beams, a large number of researches have been conducted in the area of static deflection, pull-in voltage, frequency and dynamic responses as follows.

Nayfeh *et al.* (2007), Abdel-Rahman *et al.* (2002), Nayfeh and Younis (2005), Younis and Nayfeh (2003) present a comprehensive theoretical model for a clamped-clamped micro beam under electrostatic excitation, and analyze its static and dynamic behaviors in different works. They solve the equations of motion using direct

∗Corresponding author, Assistant Professor
E-mail: zamanian@khu.ac.ir
[a]M.Sc. Graduate, E-mail: polouei@gmail.com
[b]Assistant Professor, E-mail: ali.hosseini@khu.ac.ir

ISSN: 1225-4568 (Print), 1598-6217 (Online)

perturbation method or discretize the equations of motion using Galerkin method and solve them using numerical shooting method. They observe a softening behavior due to electrostatic actuation and a hardening behavior due to nonlinear mid plane stretching term. The static and dynamic behavior of an electrostatically actuated micro-cantilever beam have been examined by Lizhoung and Xiaoli (2007). They only considered the nonlinear terms due to electrostatic forces and used perturbation approach to solve the nonlinear equations. A similar micro beam which is separated from the fixed plane by relatively larger gap has been studied by Chaterjee and Pohit (2009). They showed that the geometrical nonlinearities due to shortening effect play a notable part when pull-in transpires. Rasekh and Khadem (2011) studied dynamic response of an electrostatically excited nano-cantilever as numeric and indicated that the softening effect is due to nonlinear inertia term as opposed to hardening effect which is because of nonlinear curvature term. Pull-in features of a reinforced CNT has been analytically examined by taking geometric nonlinearity, thermally-corrected Casimir force and surface effect into account and the ultimate outcomes indicate that the pull-in voltage grows as the volume fraction of CNTs rises (Yang and Wang 2016). A revised deformation function has been proposed by Huang *et al.* (2014), which takes both of tilted and curled bending into consideration and the results give clear indication of accuracy improvement of pull-in voltage analytical solution. Najar *et al.* (2015) have analyzed the DC voltage excited capacitive nanoactuator with a focus on small scale effect on the nonlinear static and dynamic responses. They considered Casimir and von der Waals intermolecular forces, and revealed that the nonlinear midplane stretching term has significant influence on the results of pull-in. Employing the strain gradient theory, the static deflection and pull-in voltage of a micro cantilever, which is excited electrostatically, have been surveyed and it is inferred that the gap between theory and practice can be bridged by means of strain gradient theory (Rahaeifard and Ahmadian 2015). Aboelkassem *et al.* (2010) state some recommendations in order to improve the design of the current micro sensors by modelling a bio-mass sensor with the assistance of a cantilever beam with a proof mass attached to its tip. Static and dynamic responses, pull-in voltage, rate sensitivity, resolution, bandwidth, and shock resistance of a gyroscope, which has been modelled by a tipped patch micro-cantilever operating in the flexural-flexural mode, have been investigated by Rasekh and Khadem (2013). The electro-elasto-static and electro-elasto-dynamic behaviors of a nonlinear size-dependent MEMS have come under scrutiny. The proposed model is excited by DC and AC voltages and it considers electrical/displacement nonlinearities (Ghayesh *et al.* 2015). An effective length of the flexible pads has been determined by means of shooting method to close the gap between theoretical and experimental analysis by Bataineh and Younis (2015). Zamanian and Karimiyan (2015) have studied nonlinear vibration of a $\perp$ shaped mass attached to a clamped-clamped micro beam under electrostatic actuation considering the effect of stretching. The examination of a clamped-clamped micro beam dynamic behavior, actuated near its third and fifth natural frequencies has led to a conclusion that the dynamic amplitude of the partial electrode, excited with two-phase shift sources of voltage, is more than a single-voltage-source full electrode (Masri and Younis 2015). The nonlinear dynamic behavior modelling of a resonator presents that several complicated nonlinear behaviors, such as quasiperiodic motion, torus bifurcations, coexistence of attractors, and modulated chaotic attractors, may exist (Younis 2015). A carbon nanotube cantilever is studied by Kim and Lee (2015) where super harmonic, subharmonic and primary resonances under AC and DC harmonic actuation are taken into consideration. Surface effects and nonlinear curvature have been incorporated into a typical model of nano-cantilever switches by Wang and Wang (2015), and the outcomes indicate that attributes such as nonlinear curvature and surface elasticity stiffen the cantilever beam, as opposed to the positive residual surface stress which softens it. Rayleigh-Ritz approach, premised upon Lagrange and Newton Harmonic Balance approaches, has been employed to investigate the nonlinear vibration behavior of single and double tapered cantilever beams by Sun *et al.* (2016).

Several studies have focused on multi-layer micro beams. A two layered clamped-clamped micro beam has been modelled using finite-difference method by Nie *et al.* (2006). They proposed the measurement of material properties of a layer deposited on the micro beam by pull-in method. Multilayered cantilever and clamped-clamped beams are simulated in a similar study and solving the nonlinear equations numerically suggests that the obtained outcomes can be helpful in the optimization process of MEMS switch designs or other actuators (Rezazadeh 2008). A new remote temperature sensor is proposed by Rezazadeh *et al.* (2012), in which thermo-mechanical behavior is studied with the help of numerical and perturbation approach. The acquired results demonstrate that the rise of natural frequency alongside the temperature relaxation time decline cause the sensor operates more dynamically and sensitively. The effect of piezoelectric layer on the mechanical behavior of an electrostatically actuated micro beam have been considered by Raeisifard (2014) and Zamanian and Khadem (2010.)

A number of studies on the viscoelastic micro beams or a micro beam coated by viscoelastic layer have been reported. The dynamic response of an electrostatically clamped-clamped viscoelastic micro beams subjected to nonlinear stretching effect has been studied by Zamanian *et al.* (2010) and Fu *et al.* (2009). Chitsaz and Jalali (2015) study the nonlinear dynamic response of a nanocomposite clamped-clamped Euler-Bernoulli viscoelastic micro beam under simultaneous electrostatic and piezoelectric actuations by means of Galerkin and perturbation methods. They demonstrate that in electrostatic excitation, hardening effect takes place for the lower range of DC voltage. On the contrary, softening effect is observed as the DC voltage increases. Nonlinear free vibrations of a viscoelastic microcantilever subjected to the nonlinear shortening effect have been presented by Shooshtari *et al.* (2012). They consider the micro beam under piezoelectric actuation and

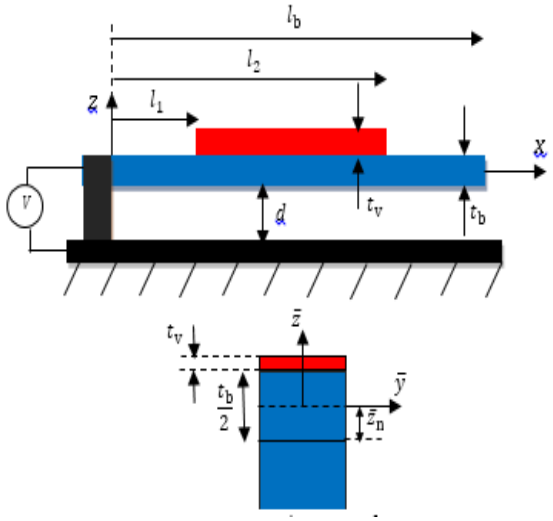

Fig. 1 Micro beam configuration

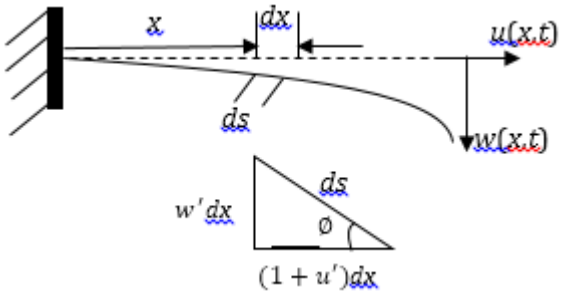

Fig. 2 Deflected micro beam

state that the damping coefficient and the piezoelectric layer length play vital roles in system response. In a similar study (Hoseini *et al.* 2014), the nonlinear-forced vibrations of the mentioned model have been investigated. In this work, the Multiple Scale method is utilized for the frequency response consideration and the required outcomes represent that both softening and the maximum vibration amplitude attributes are significantly influenced by piezoelectric layer length factor.

Recently the cantilever micro beam coated by a viscoelastic patch has been attended as a main element of gas and mass sensors (Boudjiet *et al.* 2015, Dufour *et al.* 2007 and Younis and Alsaleem 2009). In this configuration, the gas or mass is absorbed by viscoelastic layer. When this configuration is excited by electrostatic actuation then the amount or existence of mass or gas is detected by the process which is mentioned at the second paragraph of this section. The length and thickness of viscoelastic layer have main effect on the sensitivity and performance of these devices. Poloei *et al.* (2015) study a modification on the geometry of the viscoelastic patch when the sensor is based on the change on capacitance change. They determine the optimum length and thickness for viscoelastic layer by the assumption that the viscoelastic layer mass is constant.

This work can be viewed as significant development of the last mentioned paper. The main distinguishing feature of this work is that the applied voltage between the micro beam and the set plate is combination of DC and AC voltage, as opposed to the previous work which was solely premised upon DC voltage. In other words, the sensor performance is mainly based on resonance frequency in this work, in contrast with the preceding paper which is based on capacitance. It should be noted that the structural damping of the viscoelastic layer is taken into consideration in the dynamic motion equation due to the vibration caused by AC voltage. By assuming that the volume of deposited layer is constant, the variation of frequency response for different lengths and thicknesses of the viscoelastic layer have been founded. The ultimate objective of the current study is to obtain the optimum length and thickness which result in the minimum amount of nonlinear resonance variation. The considered nonlinear terms, in this work, are composed of geometrical, inertia, electrostatic and viscoelastic nonlinearities. Viscoelastic layer abides by the Kelvin-Voigt model. The motion equation is then discretized by Galerkin method. It is noteworthy that the mode shapes of a viscoelastic patched micro beam have been exploited to discretize the motion equation. The multiple scale perturbation method has been applied to solve the discrete dynamic equation. The analytical perturbation solution is verified by comparing the analytical perturbation solution with numerical solution.

2. Problem statement and formulation

Fig. 1 indicates a typical micro beam configuration. As is seen, the fixed plate is set opposite the movable micro beam, and the viscoelastic layer is patched on the micro beam. As the voltage is applied to the set plate and the micro beam, the micro beam moves towards the plate.

Two coordinate systems have been employed, inertial coordinate system $(\boldsymbol{x}, \boldsymbol{z})$ and local coordinate system $(\bar{\boldsymbol{x}}, \bar{\boldsymbol{z}})$, as so to expand the motion equations. Assuming that $\boldsymbol{u}$ and $\boldsymbol{w}$ are the displacement along the longitudinal axis $(\boldsymbol{x})$ and the transverse axis $(\boldsymbol{z})$, the correlation between the deflected elements displacements $(\boldsymbol{ds})$ can be formulated as follows.

$$e = \frac{ds - dx}{dx} = \sqrt{(1+u')^2 + w'^2} - 1$$
$$\cos\theta = \frac{1+u'}{1+e}, \quad \sin\theta = \frac{w'}{1+e}, \quad \theta = \arctan g \frac{w'}{1+u'} \tag{1}$$

Where θ is the rotation angle, e is the longitudinal strain of the neutral axis, and ds is the deflected element length.

Considering the assumption of shortening effect, the cross section strain $(\bar{\varepsilon})$ is calculated as follows.

$$\bar{\varepsilon} = -\kappa \bar{z} \quad , \quad \kappa = \theta' \tag{2}$$

Where $\bar{z}$ is the distance from the neutral axis, and κ is the bending curvature in xz plane.

Computing the derivative of θ (in Eq. (1)) with respect to x results in bending curvature, by means Taylor series

$$\kappa = \theta' = w'' - w''u' - w'u'' - w''w'^2 + \ldots \tag{3}$$

The neutral axis coincides with midline of the micro beam cross section at the parts which are not covered by the viscoelastic layer. It is worth remembering that the distance of the neutral axis from the micro beam middle layer is presented by $\bar{z}_n$ in the patched parts, as shown in Fig. 1.

$$\begin{aligned}&\bar{z}dA = 0 \Rightarrow \\ &\int_A \int_{\frac{-t_b}{2}-\bar{z}_n}^{\frac{t_b}{2}-\bar{z}_n} \bar{z}\,(\mathrm{w}_b \mathrm{d}\bar{z}) + \int_{\frac{t_b}{2}-\bar{z}_n}^{\frac{t_b}{2}-\bar{z}_n+t_v} \bar{z}\,(\frac{E_v}{E_b}\mathrm{w}_b \mathrm{d}\bar{z}) = 0 \\ &\Rightarrow \quad \bar{z}_n = \frac{E_v t_v (\mathrm{t}_v + \mathrm{t}_b)}{2(\mathrm{t}_b \mathrm{E}_b + \mathrm{t}_v \mathrm{E}_v)}\end{aligned} \tag{4}$$

Where t_b and t_v are the thicknesses and E_b and E_v are the elasticity modules of the micro beam and viscoelastic layer respectively (Mahmoodi *et al.* 2007).

The stress-strain relationship of the micro beam is formulated with respect to Hook's law as Eq. (5)

$$\sigma_b = E_b \bar{\varepsilon} \tag{5}$$

Where σ_b is perceived as the micro beam stress.

The viscoelastic layer stress and strain equations of the Kelvin-Voit model can be formulated as Eq. (6) (Mahmoodi *et al.* 2008)

$$\begin{aligned}&\sigma_v = \sigma_{v_c} + \sigma_{v_{nc}} \\ &\sigma_{v_c} = E_v \bar{\varepsilon} \quad , \quad \sigma_{v_{nc}} = C\dot{\bar{\varepsilon}}\end{aligned} \tag{6}$$

Where σ_v is the axial stress of the viscoelastic layer, C is the viscoelastic coefficient, σ_{v_c} is the conservative term, and $\sigma_{v_{nc}}$ is the non-conservative term.

The longitudinal and transverse motion equations are calculated by the employment of Hamilton principle. To do so, the kinetic and potential energies must be determined in the first place.

The kinetic energy can be formulated as Eq. (7) with the ignorance of rotational inertia.

$$T = \frac{1}{2}\int_0^l m(x)\left(\dot{u}^2 + \dot{w}^2\right)dx \tag{7}$$

The above-mentioned derivatives are considered with respect to time, and another point is that micro beam length is l. Mass per unit of length is calculated as follows

$$\begin{aligned}&m(x) = w_b\left(\rho_b t_b + \left(H_{l_1} - H_{l_2}\right)\rho_v t_v\right) \\ &H_{l_i} = H(x - l_i) = \begin{cases}1 & x \geq l_i \\ 0 & x \leq l_i\end{cases} \quad i = 1,2\end{aligned} \tag{8}$$

Where w_b is width of the micro beam and the viscoelastic layer, ρ_b is the micro beam density, and ρ_v is the viscoelastic layer density.

The integration of the micro beam strain energy and the viscoelastic layer conservative strain energy results in the conservative strain energy of the micro system as formulated in Eq. (9).

$$\begin{aligned}U_c = &\int_{V_b}\int_0^{\bar{\varepsilon}} \sigma_b\, d\bar{\varepsilon}\, dV_b + \int_{V_v}\int_0^{\bar{\varepsilon}} \sigma_{v_c}\, d\bar{\varepsilon}\, dV_v = \\ &\int_0^l \int_{-\frac{t_b}{2}-\bar{z}_n}^{\frac{t_b}{2}-\bar{z}_n} \int_0^{\bar{\varepsilon}} \left(H_{l_1} - H_{l_2}\right)\sigma_b d\,\bar{\varepsilon}\, w_b\, d\bar{z}\, dx + \\ &\int_0^l \int_{-\frac{t_b}{2}}^{\frac{t_b}{2}} \int_0^{\bar{\varepsilon}} H_{l_2}\sigma_b\, d\,\bar{\varepsilon}\, w_b\, d\bar{z}\, dx + \\ &\int_0^l \int_{\frac{t_b}{2}-\bar{z}_n}^{\frac{t_b}{2}-\bar{z}_n+t_p} \int_0^{\bar{\varepsilon}} \left(H_{l_1} - H_{l_2}\right)(\sigma_v)_c\, d\,\bar{\varepsilon}\, w_b\, d\bar{z}\, dx\end{aligned} \tag{9}$$

Where dV_b and dV_v are the differential volumes of the micro beam and the viscoelastic layer respectively. The conservative strain energy can be calculated by the application of the above-mentioned equations.

$$\begin{aligned}&U_c = \frac{1}{2}\int_0^l C_\eta(x)\kappa^2 dx \\ &U_c = \frac{1}{2}\int_0^l C_\eta(x)\left(w''-w''u'-w'u''-w''w'^2\right)^2 dx\end{aligned} \tag{10}$$

Where $C_\eta(x)$ is the flexural stiffness and can be formulated as follows

$$\begin{aligned}&C_\eta(x) = \left(1-H_{l_1}\right)E_b I_b + \left(H_{l_1} - H_{l_2}\right)E_b \bar{I}_b \\ &+\left(H_{l_1} - H_{l_2}\right)E_v I_v + H_{l_2} E_b I_b \\ &I_b = \frac{w_b t_b^3}{12} \quad , \quad \bar{I}_b = \frac{w_b t_b^3}{12} + w_b t_b \bar{z}_n^2 \\ &I_v = w_v\left(t_v \bar{z}_n^2 - \left(t_v^2 + t_b t_v\right)\bar{z}_n\right) + \\ &\frac{w_v}{3}\left(t_v^3 + \frac{3}{2}t_b t_v^2 + \frac{3}{4}t_b^2 t_v\right)\end{aligned} \tag{11}$$

The electrostatic potential energy is calculated as follows

$$Q_v = -\frac{1}{2}\varepsilon_0 w_b (\mathrm{v}_{dc} + \mathrm{v}_{ac}\cos\Omega t)^2 \int_0^l \frac{1}{d-w}dx \tag{12}$$

Where ε_0 is the Dielectric constant and d is the gap between set plate and micro beam, v_{dc} and v_{ac} are DC and AC voltages applied between microbeam and fixed electrode plate, respectively. Moreover t is time and Ω is the frequency of AC voltage.

Virtual work, arising from non-conservative term, is calculated as follows

$$\delta W_{nc} = \int_{V_v} \sigma_{v_{nc}} \delta\bar{\varepsilon}\, dV_v \tag{13}$$

The employment of Eqs. (2)-(6) in Eq. (13) can be written as follows

$$\delta W_{nc} = \iint_A \left(H_{l_1} - H_{l_2}\right)C\bar{z}^2(\dot{\kappa})\delta(\kappa)dAdx \tag{14}$$

The utilization of Eq. (3) will result in

$$\begin{aligned}&\delta W_{nc} = \iint_A \Big(\left(H_{l_1} - H_{l_2}\right)C\bar{z}^2(\dot{\kappa}) \\ &\delta\left(w''-w''u'-w'u''-w''w'^2\right)dAdx\Big)\end{aligned} \tag{15}$$

The integration by parts application of Eq. (15) and keeping the terms up to third order result in the following equation

$$\begin{aligned}
&\delta w_{nc} = \iint_A \left(H_{l_1} - H_{l_2}\right) C\bar{z}^2 \left(\dot{\kappa}\right)'' \delta w dA dx \\
&\delta w_{nc} = \int C_\varsigma \left(\dot{w}''-\dot{w}'u'-w'\dot{u}'-\dot{w}'u''-\right. \\
&\left. w'\dot{u}''-\dot{w}'w'^2-2\dot{w}'w'w''\right)'' \delta w dx \\
&C_\varsigma = (\mathrm{H}_{l_1} - \mathrm{H}_{l_2}) C I_v
\end{aligned} \tag{16}$$

Since the shortening effect exists in a cantilever beam, in which the longitudinal load is ignored (Nayfeh and Pai 2004), the axial strain (e), in Eq. (1), is zero and the shortening effect is formulated as follows

$$e = \sqrt{(1+u')^2 + w'^2} - 1 = 0 \tag{17}$$

The Hamilton principle is defined as Eq. (18).

$$\begin{aligned}
&\delta \int_{t_1}^{t_2} (T - U_c - Q_v + \lambda G) dt + \int_{t_1}^{t_2} \delta W_{nc} dt = 0 \\
&G = (1+u')^2 + w'^2 - 1
\end{aligned} \tag{18}$$

Where λ is utilized to take the shortening effect into account with the assistance of G which is the constraint arising from the inextentional attribute of neutral axis.

The longitudinal and transverse governing motion equations are formulated by means of Hamilton principle as follows

$$\begin{aligned}
&-\left(C_\eta(\mathrm{x})\,\mathrm{w}''^2\right)' + \left(\lambda(1+u')\right)' + \\
&\left(C_\eta(x) w' w''\right)'' - m(x)\ddot{u} = 0 \qquad (a) \\
&-[2C_\eta(\mathrm{x})\,\mathrm{w}'\mathrm{w}''^2 + C_\eta\,\mathrm{w}''\mathrm{u}'']' + [\lambda\,\mathrm{w}']' + \\
&[-C_\eta(\mathrm{x})\,\mathrm{w}'' + 2C_\eta(\mathrm{x})\,\mathrm{w}''w'^2 + \\
&2C_\eta(\mathrm{x})\,\mathrm{w}''\mathrm{u}' + C_\eta(\mathrm{x})\,\mathrm{w}'\mathrm{u}'']'' - \\
&\mathrm{m(x)}\,\ddot{\mathrm{w}} = \frac{1}{2}\varepsilon_0 w_b \frac{(\mathrm{v}_{dc} + \mathrm{v}_{ac}\cos\Omega t)^2}{(\mathrm{d}+w)^2} \qquad (b)
\end{aligned} \tag{19}$$

Solving Eq. (17) for u' and its Taylor series, it can be finalized that

$$u' = -\frac{1}{2}w'^2 \;\Rightarrow\; u(x,t) = -\frac{1}{2}\int_0^x w'^2 dx \tag{20}$$

By application of integral, with respect to x and in the range of x to l, in Eq. (19(a)), and the boundary conditions employment in the free end of the micro beam, the following outcome can be obtained

$$\lambda = C_\eta(x) w''^2 - \left[C_\eta(s) w' w''\right]' + \int_l^x m(x)\ddot{u} dx + \ldots \tag{21}$$

The insertion of Eqs. (20)-(21) into Eq. (19(b)) results in

$$\begin{aligned}
&m(x)\ddot{w} + \left(C_\eta(x) w''\right)'' + \left(w'\left(C_\eta(\mathrm{x})\,\mathrm{w}'\mathrm{w}''\right)'\right)' \\
&+\left(w'\int_l^x \left(m(\mathrm{x})\int_0^x \left(w'\ddot{w}' + \dot{w}'^2\right)dx\right)dx\right)' + \\
&\left(C_\varsigma(\mathrm{x})\left(\dot{w}'' + \frac{1}{2}\dot{w}'w'^2 + w'\dot{w}'w'\right)\right)'' \\
&+\frac{1}{2}\varepsilon_0 w_b \frac{(V_{dc} + v_{ac}\cos\Omega t)^2}{(d+w)^2} = 0
\end{aligned} \tag{22}$$

The micro cantilever beam boundary conditions are

$$\begin{aligned}
&w\big|_{x=0} = 0, \quad w'\big|_{x=0} = 0, \\
&w''\big|_{x=l} = 0, \quad w'''\big|_{x=l} = 0
\end{aligned} \tag{23}$$

In Eq. (22), the first two terms show the micro beam linear equation, the third term represents geometric nonlinearities, the fourth term indicates the inertia nonlinearity, the fifth term presents the viscoelastic layer effect, and the last term specifies the nonlinear electrostatic force which is in agreement with Chaterjee and Pohit (2009) if the viscoelastic terms are neglected.

The following changes in variables have been defined so as to obtain the dimensionless governing motion equation.

$$\hat{W} = -\frac{W}{d}, \quad x = \frac{x}{l}, \quad \hat{t} = \left(\frac{t}{l^2}\right)\sqrt{\frac{E_b I_b}{\rho_b A_b}} \tag{24}$$

Omitting the ^ sign of the variables for the sake of simplicity, the non-dimensional governing motion equation and boundary conditions can be formulated as follows

$$\begin{aligned}
&m(x)\ddot{w} + \left(H_1(x) w''\right)'' + \\
&\alpha_1\left(w'\left(H_1(x) w' w''\right)'\right)' + \\
&\alpha_1\left(w'\int_1^x \left(m(\mathrm{x})\int_0^x \left(w'\ddot{w}' + \dot{w}'^2\right)dx\right)dx\right)' + \\
&\alpha_2\left(H_2(\mathrm{x})\dot{w}''\right)'' + \\
&\alpha_1\alpha_2\left(H_2(\mathrm{x})\left(\frac{1}{2}\dot{w}'w'^2 + \dot{w}'w'w'\right)\right)'' = \\
&\frac{\alpha_3(V_{dc} + v_{ac}\cos\Omega t)^2}{(1-w)^2}
\end{aligned} \tag{25}$$

$$w\big|_{x=0} = 0, \quad w'\big|_{x=0} = 0, \quad w''\big|_{x=1} = 0, \; w'''\big|_{x=1} = 0$$

Where

$$H_{\frac{l_i}{l}} = Heaviside\ function\left(x - \frac{l_i}{l}\right) = \begin{cases} 1 & x \geq \frac{l_i}{l} \\ 0 & x \leq \frac{l_i}{l} \end{cases} \quad i = 1,2$$

$$\begin{aligned}
H_1(x) = &\left(1 - H_{l_1/l}\right) + \frac{\bar{I}_b}{I_b}\left(H_{l_1/l} - H_{l_2/l}\right) + \\
&\frac{E_v I_v}{E_b I_b}\left(H_{l_1/l} - H_{l_2/l}\right) + H_{l_2/l}
\end{aligned}$$

$$H_2(\mathrm{x})=\left(H_{l_1/l}-H_{l_2/l}\right)$$

$$m(x)=\left(1+\left(H_{l_1/l}-H_{l_2/l}\right)\frac{\rho_v t_v}{\rho_b t_b}\right) \tag{26}$$

$$\alpha_1=\left(\frac{d}{l}\right)^2,\alpha_2=\frac{CI_v}{l^2\sqrt{\rho_b A_b E_b I_b}},\alpha_3=\frac{6\varepsilon_0 l^4}{E_b t_b^3 d^3}$$

Where α_1 , α_2 and $\alpha_3 V_e^2$ are the dimensionless variables.

The static deflection equation is obtained by the ignorance of time derivatives terms in Eq. (25).

$$\left(H_1(x)w_s''\right)''+\alpha_1\left(w_s'\left(H_1(x)w_s'w_s''\right)'\right)'=\frac{\alpha_3 V_{dc}^2}{(1-w_s)^2} \tag{27}$$

The above equation has been solved by utilizing three mode shapes of a uniform beam as the comparison function by poloei *et al*. (2015).

3. Dynamic response of the primary resonance actuation

w can be perceived as the integration of dynamic deflection $(w_d(x,t))$ and static deflection $(w_s(x))$ as follows (Chaterjee and Pohit 2009)

$$w(x,t)=w_{\mathrm{d}}(x,t)+w_{\mathrm{s}}(x) \tag{28}$$

Inserting Eq. (28) into governing motion equation, omitting the static deflection terms, and expanding the electrostatic excitation up to third order result in

$$\begin{aligned}
&\mathrm{m}(\mathrm{x})\ddot{\mathrm{w}}_{\mathrm{d}}+\left(\mathrm{H}_1(\mathrm{x})\mathrm{w}_{\mathrm{d}}''\right)''+\\
&\alpha_1\left(\mathrm{w}_{\mathrm{d}}'\left(\mathrm{H}_1(\mathrm{x})\left(\mathrm{w}_{\mathrm{s}}'+\mathrm{w}_{\mathrm{d}}'\right)\left(\mathrm{w}_{\mathrm{s}}''+\mathrm{w}_{\mathrm{d}}''\right)\right)'\right)'+\\
&\alpha_1\left(\mathrm{w}_{\mathrm{s}}'\left(\mathrm{H}_1(\mathrm{x})\mathrm{w}_{\mathrm{s}}'\mathrm{w}_{\mathrm{d}}''+\mathrm{H}_1(\mathrm{x})\mathrm{w}_{\mathrm{s}}''\mathrm{w}_{\mathrm{d}}'+\right.\right.\\
&\left.\left.\mathrm{H}_1(\mathrm{x})\mathrm{w}_{\mathrm{d}}''\mathrm{w}_{\mathrm{d}}'\right)'\right)+\alpha_1\left(\left(\mathrm{w}_{\mathrm{s}}'+\mathrm{w}_{\mathrm{d}}'\right)\times\right.\\
&\left.\int_1^{\mathrm{x}}\mathrm{m}(\mathrm{x})\left(\int_0^{\mathrm{x}}\left(\ddot{\mathrm{w}}_{\mathrm{d}}'\left(\mathrm{w}_{\mathrm{s}}'+\mathrm{w}_{\mathrm{d}}'\right)+\dot{\mathrm{w}}_{\mathrm{d}}'^2\right)\mathrm{dx}\right)\mathrm{dx}\right)'\\
&+\alpha_2\left(\mathrm{H}_2(\mathrm{x})\dot{\mathrm{w}}_{\mathrm{d}}''\right)''+\alpha_1\alpha_2\left(\mathrm{H}_2(\mathrm{x})\times\right.\\
&\left.\left(\frac{1}{2}\dot{\mathrm{w}}_{\mathrm{d}}''\left(\mathrm{w}_{\mathrm{s}}'^2+\mathrm{w}_{\mathrm{d}}'^2\right)+\right.\right.\\
&\left.\left.\dot{w}_d\left(w_s''+w_d''\right)\left(w_s'+w_d'\right)\right)\right)''\\
&=\frac{\alpha_3\left(2V_{dc}v_{ac}\cos\Omega t+\left(v_{ac}\cos\Omega t\right)^2\right)}{(w_s-1)^2}-\\
&\frac{2\alpha_3\left(V_{dc}+v_{ac}\cos\Omega t\right)^2}{(w_s-1)^3}w_d+\\
&\frac{3\alpha_3\left(V_{dc}+v_{ac}\cos\Omega t\right)^2}{(w_s-1)^4}w_d^2-\\
&\frac{4\alpha_3\left(V_{dc}+v_{ac}\cos\Omega t\right)^2}{(w_s-1)^5}w_d^3
\end{aligned} \tag{29}$$

The Galerkin method is employed to discretize the governing motion equation. To do so, the non-uniform mode shapes have been utilized as comparison function.

4. Non-uniform linear mode shapes

The linear mode shapes of the non-uniform micro beam can be calculated by solving the homogeneous dimensionless equation with the consideration of viscoelastic geometric effect as follows

$$m(x)\frac{\partial^2 w}{\partial t^2}+\frac{\partial^2}{\partial x^2}\left(H_1(x)\frac{\partial^2 w}{\partial x^2}\right)=0 \tag{30}$$

By the assumption that $w(x,t)=\varphi(x)e^{i\omega t}$

$$-\omega^2 m(x)\varphi(x)+\frac{\partial^2}{\partial x^2}\left[H_1(x)\frac{\partial^2\varphi(x)}{\partial x^2}\right]=0 \tag{31}$$

Where $\varphi(x)$ the non-uniform linear mode is shape, and ω is the natural frequency.

Eq. (31) is composed of three principal parts. The first part is $\left[0,\frac{l_1}{l}\right)$ without the viscoelastic layer, the second part is $\left(\frac{l_1}{l},\frac{l_2}{l}\right)$ which has been coated with viscoelastic layer, and the last part is $\left(\frac{l_2}{l},1\right]$ in which there is no viscoelastic layer as well.

$$\begin{cases}
-\omega^2\varphi(x)+\dfrac{\partial^4\varphi(x)}{\partial x^4}=0, 0\le x<\dfrac{l_1}{l}\\
-\left(1+\dfrac{\rho_v t_v}{\rho_b t_b}\right)\omega^2\varphi(x)+\\
\left(\dfrac{\bar{I}_b}{I_b}+\dfrac{E_v I_v}{E_b I_b}\right)\dfrac{\partial^4\varphi(x)}{\partial x^4}=0 \quad , \dfrac{l_1}{l}<x<\dfrac{l_2}{l}\\
-\omega^2\varphi(x)+\dfrac{\partial^4\varphi(x)}{\partial x^4}=0, \dfrac{l_2}{l}<x\le 1
\end{cases} \tag{32}$$

Eq. (32) is solved as follows, assuming that $\varphi(x)$ consists of $W_1(x)$, $W_2(x)$, and $W_3(x)$.

$$\begin{cases}
W_1(x)=C_1\cosh(\beta_1 x)+C_2\sinh(\beta_1 x)+\\
C_3\cos(\beta_1 x)+C_4\sin(\beta_1 x)\\
W_2(x)=C_5\cosh(\beta_2 x)+C_6\sinh(\beta_2 x)+\\
C_7\cos(\beta_2 x)+C_8\sin(\beta_2 x)\\
W_3(x)=C_9\cosh(\beta_3 x)+C_{10}\sinh(\beta_3 x)+\\
C_{11}\cos(\beta_3 x)+C_{12}\sin(\beta_3 x)
\end{cases} \tag{33}$$

Where

$$\beta_{1n}=\beta_{3n}=\sqrt{\omega_n},\beta_{2n}=\left(\frac{1+\left(\frac{\rho_p t_p}{\rho_b t_b}\right)}{\left(\frac{\bar{I}_b}{I_b}+\frac{E_p I_p}{E_b I_b}\right)}\omega_n^{\,2}\right)^{\frac{1}{4}} \tag{34}$$

The constant coefficients of C_i are obtained from the micro cantilever boundary conditions, $W_1(x)$ and $W_2(x)$, and the succeeding continuity conditions.

$$\begin{aligned}
&W_1\big|_{x=0}=0, W_1'\big|_{x=0}=0, W_3''\big|_{x=1}=0, W_3'''\big|_{x=1}=0\\
&W_1\Big|_{x=\frac{l_1}{l}}=W_2\Big|_{x=\frac{l_1}{l}},\ \frac{\partial W_1}{\partial x}\Big|_{x=\frac{l_1}{l}}=\frac{\partial W_2}{\partial x}\Big|_{x=\frac{l_1}{l}}\\
&\frac{\partial^2 W_1}{\partial x^2}\Big|_{x=\frac{l_1}{l}}=K_1\frac{\partial^2 W_2}{\partial x^2}\Big|_{x=\frac{l_1}{l}}\\
&\frac{\partial^3 W_1}{\partial x^3}\Big|_{x=\frac{l_1}{l}}=K_1\frac{\partial^3 W_2}{\partial x^3}\Big|_{x=\frac{l_1}{l}}\\
&W_2\Big|_{x=\frac{l_2}{l}}=W_3\Big|_{x=\frac{l_2}{l}},\ \frac{\partial W_2}{\partial x}\Big|_{x=\frac{l_2}{l}}=\frac{\partial W_3}{\partial x}\Big|_{x=\frac{l_2}{l}}\\
&K_1\frac{\partial^2 W_2}{\partial x^2}\Big|_{x=\frac{l_2}{l}}=\frac{\partial^2 W_3}{\partial x^2}\Big|_{x=\frac{l_2}{l}}\\
&K_1\frac{\partial^3 W_2}{\partial x^3}\Big|_{x=\frac{l_2}{l}}=\frac{\partial^3 W_3}{\partial x^3}\Big|_{x=\frac{l_2}{l}}
\end{aligned} \tag{35}$$

Where $K_1=\frac{\bar{I}_b}{I_b}+\frac{E_v I_v}{E_b I_b}$.

By determining the above-mentioned constant coefficients, the non-uniform linear mode shapes are acquired as follows

$$\begin{aligned}
\varphi(x)=&\left(1-H_{l_1/l}\right)W_{1n}(x)+\\
&\left(H_{l_1/l}-H_{l_2/l}\right)W_{2n}(x)+H_{l_2/l}W_{3n}(x)
\end{aligned} \tag{36}$$

Now it is assumed that $w_d=P(t)\varphi(x)$, where $P(t)$ is time coordinate of the system response. By substituting this assumption into Eq. (29) and multiplying the outcome by $\varphi(x)$, and integrating along the length of microbeam the governing equation motion at primary resonance case will be as follows

$$\begin{aligned}
&k_l^I\left(\frac{d^2}{dt^2}P(t)\right)+\left(k_{l,0}^E+k_{l,1}^E\left(v_{ac}\cos\Omega t\right)+\right.\\
&\left.k_{l,2}^E\left(v_{ac}\cos\Omega t\right)^2+k_l^G\right)\left(P(t)\right)+\\
&\left(k_q^G+k_{q,0}^E+k_{q,1}^E\left(v_{ac}\cos\Omega t\right)+\right.\\
&\left.k_{q,2}^E\left(v_{ac}\cos\Omega t\right)^2\right)\left(P(t)\right)^2+\\
&\left(k_c^G+k_{c,0}^E+k_{c,1}^E\left(v_{ac}\cos\Omega t\right)+\right.\\
&\left.k_{c,2}^E\left(v_{ac}\cos\Omega t\right)^2\right)\left(P(t)\right)^3\\
&-k_{q1}^I\left(\frac{d^2}{dt^2}P(t)\right)\left(P(t)\right)-k_c^I\left(\frac{d^2}{dt^2}P(t)\right)\left(P(t)\right)^2\\
&-k_{q2}^I\left(\frac{d}{dt}P(t)\right)^2-k_c^I\left(\frac{d}{dt}P(t)\right)^2\left(P(t)\right)+\\
&k_l^v\left(\frac{d}{dt}P(t)\right)+\left(k_{0,1}^E\right)v_{ac}\cos\Omega t+\\
&\left(k_{0,2}^E\right)\left(v_{ac}\cos\Omega t\right)^2=0
\end{aligned} \tag{37}$$

Where k_l^I, $(k_{l,0}^E, k_{l,1}^E, k_{l,2}^E)$ and k_l^G arise from the linear inertia, electrostatic, and curvature respectively, $k_q^I=k_{q1}^I+k_{q2}^I$, $(k_{q0}^E, k_{q1}^E, k_{q2}^E)$ and k_q^G are arisen from second order non-linear inertia, electrostatic and curvature, and k_c^I, $(k_{c0}^E, k_{c1}^E, k_{c2}^E)$ and k_c^G arise from the third order non-linear inertia, electrostatic and curvature. $k_{0,1}^E$ and $k_{0,2}^E$are the electrostatic excitation effect, and k_l^v is the linear viscoelastic effect. These coefficients are listed in Appendix A.

5. Perturbation theory

Eq. (37) can be solved by means of multiple scale method of perturbation theory assuming that the non-linear terms have lower orders in comparison with the linear ones.

$$\begin{aligned}
&P(t)=\varepsilon P_1(T_0,T_1,T_2)+\varepsilon^2 P_2(T_0,T_1,T_2)+\\
&\varepsilon^3 P_3(T_0,T_1,T_2)
\end{aligned} \tag{38}$$

Where $T_0=t$, $T_1=\varepsilon t$, and $T_2=\varepsilon^2 t$ are the time scales, and ε is the Bookkeeping parameter which demonstrates the order of the expressions. Computing the function derivatives with the assistance of the chain rule will result in

$$\begin{aligned}
&\frac{d}{dt}=D_0+\varepsilon D_1+\varepsilon^2 D_2\\
&\frac{d^2}{dt^2}=D_0^2+2\varepsilon D_0 D_1+\varepsilon^2\left(2D_0 D_2+D_1^2\right)
\end{aligned} \tag{39}$$

Where D_n is $\frac{\partial}{\partial T_n}; n=0,1,2.$

The orders of the viscoelastic damping and the AC actuation are viewed ε^2 and ε^3 respectively so as to strike a balance between nonlinear terms, damping, and excitation. Furthermore, considering the orders as ε^2 and ε^3 accounts for all the existing terms in the equation and makes the problem solvable.

Order (ε^1)

$$\frac{\partial^2}{\partial T_0^{\,2}}P_1(T_0,T_1,T_2)+\frac{k_{l,0}^E+k_l^G}{k_l^I}P_1(T_0,T_1,T_2)=0 \tag{40}$$

Order (ε^2)

$$\begin{aligned}
&\frac{\partial^2}{\partial T_0^{\,2}}P_2(T_0,T_1,T_2)+\frac{k_{l,0}^E+k_l^G}{k_l^I}P_2(T_0,T_1,T_2)=\\
&-\frac{k_{q2}^I}{k_l^I}\left(\frac{\partial}{\partial T_0}P_1(T_0,T_1,T_2)\right)^2-
\end{aligned}$$

$$\frac{k_{q1}^{I}}{k_{l}^{I}}P_1(T_0,T_1,T_2)\frac{\partial^2}{\partial T_0^{\,2}}P_1(T_0,T_1,T_2)-$$
$$2\frac{\partial^2}{\partial T_1\partial T_0}P_1(T_0,T_1,T_2)- \quad (41)$$
$$\frac{k_{q,0}^{E}+k_{q}^{G}}{k_{l}^{I}}\left(P_1(T_0,T_1,T_2)\right)^2$$

Order (ε^3)

$$-\frac{\left(k_{c,0}^{E}+k_{c}^{G}\right)}{k_{l}^{I}}\left(P_1(T_0,T_1,T_2)\right)^3-$$
$$2\frac{\partial^2}{\partial T_1\partial T_0}P_2(T_0,T_1,T_2)-$$
$$2\frac{k_{q1}^{I}}{k_{l}^{I}}P_1(T_0,T_1,T_2)\frac{\partial^2}{\partial T_1\partial T_0}P_1(T_0,T_1,T_2)-$$
$$\frac{2\left(k_{q,0}^{E}+k_{q}^{G}\right)}{k_{l}^{I}}P_1(T_0,T_1,T_2)P_2(T_0,T_1,T_2)-$$
$$\frac{k_{c}^{I}}{k_{l}^{I}}P_1(T_0,T_1,T_2)\left(\frac{\partial}{\partial T_0}P_1(T_0,T_1,T_2)\right)^2- \quad (42)$$
$$\frac{k_{q1}^{I}}{k_{l}^{I}}P_2(T_0,T_1,T_2)\frac{\partial^2}{\partial T_0^{\,2}}P_1(T_0,T_1,T_2)-$$
$$\frac{k_{c}^{I}}{k_{l}^{I}}\left(P_1(T_0,T_1,T_2)\right)^2\frac{\partial^2}{\partial T_0^{\,2}}P_1(T_0,T_1,T_2)-$$
$$\frac{2k_{q2}^{I}}{k_{l}^{I}}\left(\frac{\partial}{\partial T_0}P_1(T_0,T_1,T_2)\right)\frac{\partial}{\partial T_1}P_1(T_0,T_1,T_2)-$$
$$\frac{k_{l}^{v}}{k_{l}^{I}}\frac{\partial}{\partial T_0}P_1(T_0,T_1,T_2)-k_{0,1}^{E}v_{ac}\cos\Omega T_0$$

Eq. (40) can be solved as follows, assuming that $\omega=\sqrt{\frac{k_{l,0}^{E}+k_{l}^{G}}{k_{l}^{I}}}$.

$$P_1(T_0,T_1,T_2)=A(T_1,T_2)e^{i\omega t}+\bar{A}(T_1,T_2)e^{-i\omega t} \quad (43)$$

It should be noted that $A(T_1,T_2)$ is a complex function which is obtained by the solvability conditions. The insertion of Eq. (43) in Eq. (41) will lead to

$$\frac{\partial^2}{\partial T_0^{\,2}}P_2(T_0,T_1,T_2)+\omega^2P_2(T_0,T_1,T_2)=$$
$$-2\omega i\left(\frac{\partial}{\partial T_1}A(T_1,T_2)\right)e^{i\omega T_0}-$$
$$\frac{\left(-k_{q1}^{I}\omega^2-k_{q2}^{I}\omega^2+k_{q}^{G}+k_{q,0}^{E}\right)}{k_{l}^{I}}\times$$
$$\left(\left(A(T_1,T_2)\right)^2e^{2i\omega T_0}\right)+CC$$
$$-\frac{2\left(-k_{q1}^{I}\omega^2+k_{q2}^{I}\omega^2+k_{q}^{G}+k_{q,0}^{E}\right)}{k_{l}^{I}}\times \quad (44)$$
$$\left(A(T_1,T_2)\bar{A}(T_1,T_2)\right)$$

$e^{i\omega T_0}$ Coefficient has to be equaled to zero in order to omit the secular term from Eq. (44).

$$\left(\frac{\partial}{\partial T_1}A(T_1,T_2)\right)e^{i\omega T_0}+\left(\frac{\partial}{\partial T_1}\bar{A}(T_1,T_2)\right)e^{-i\omega T_0}=0 \quad (45)$$

It is implied from Eq. (45) that A has to be merely a function of T_2. The particular response of the Eq. (44) will be as follows

$$P_2(T_0,T_1,T_2)=$$
$$\frac{1}{3}\frac{\left(\left(k_{q1}^{I}+k_{q2}^{I}\right)\omega^2+k_{q}^{G}+k_{q,0}^{E}\right)}{\omega^2k_{l}^{I}}\times$$
$$\left(A(T_2)\right)^2e^{2i\omega T_0}+CC \quad (46)$$
$$\frac{-2\left(\left(-k_{q1}^{I}+k_{q2}^{I}\right)\omega^2+k_{q}^{G}+k_{q,0}^{E}\right)A(T_2)\bar{A}(T_2)}{\omega^2k_{l}^{I}}$$

Inserting P_1 and P_2 in Eq. (42), keeping the terms which result in secular expression, and with the consideration of natural frequency vibration as $\Omega=\omega+\varepsilon^2\sigma$ will be arrived in

$$\frac{\partial^2}{\partial T_0^{\,2}}P_3(T_0,T_1,T_2)+\omega^2P_3(T_0,T_1,T_2)=$$
$$\Bigg[-\frac{k_{l}^{v}\omega}{k_{l}^{I}}iA(T_2)-2\omega i\frac{d}{dT_2}A(T_2)-$$
$$\frac{1}{6k_{l}^{I\,2}\omega^2}\left(-2k_{q1}^{I\,2}\omega^4-8k_{q2}^{I\,2}\omega^4\right.$$
$$-12k_{c}^{I}k_{l}^{I}\omega^4-20k_{q2}^{I}\left(k_{q}^{G}+k_{q,0}^{E}\right)\omega^2+ \quad (47)$$
$$\left.14k_{q1}^{I}k_{q2}^{I}\omega^4-20\left(k_{q}^{G}+k_{q,0}^{E}\right)^2\right)$$
$$\left(\left(A(T_2)\right)^2\bar{A}(T_2)\right)-\frac{k_{0,1}^{E}v_{ac}}{2k_{l}^{I}}e^{i\sigma T_2}\Bigg]e^{i\omega T_0}+$$
$$CC+NST$$

Where σ is the Detuning parameter, NST stands for non-secular terms, and CC is the complex conjugate.

By inserting the polar form of the A $\left(A(T_2)=\frac{1}{2}a(T_2)e^{i\beta(T_2)}\right)$ in the secular term of the Eq. (47) the following result will be acquired

$$-\frac{k_{l}^{v}\omega}{k_{l}^{I}}-2\omega\frac{d}{dT_2}a(T_2)+$$
$$k_{0,1}^{E}v_{ac}\sin\left(\sigma T_2-\beta(T_2)\right)=0$$
$$-\frac{S}{\omega}\left(a(T_2)\right)^3+2\omega\,a(T_2)\left(\frac{d}{dT_2}\beta(T_2)\right)+ \quad (48)$$
$$k_{0,1}^{E}v_{ac}\cos\left(\sigma T_2-\beta(T_2)\right)=0$$

Whereas

$$S=\Bigg[\frac{1}{12k_{l}^{I\,2}\omega}\left(-k_{q1}^{I\,2}\omega^4-4k_{q2}^{I\,2}\omega^4-\right.$$
$$\left.6k_{c}^{I}k_{l}^{I}\omega^4-10k_{q2}^{I}\left(k_{q}^{G}+k_{q,0}^{E}\right)\omega^2+\right.$$

$$7k_{q1}^{I}k_{q2}^{I}\omega^4 - 10\left(k_q^G + k_{q,0}^E\right)^2 + 9k_l^I\left(k_c^G + k_{c,0}^E\right)\omega^2 + 11k_{q1}^I\left(k_q^G + k_{q,0}^E\right)\omega^2\Big)\Big] \quad (49)$$

Eq. (48) can be written as follows if $\gamma(T_2)$ is considered as $\gamma(T_2) = \sigma T_2 - \beta(T_2)$

$$2\omega\frac{da}{dT_2} = -\frac{k_l^v}{k_l^I}\omega a + k_{0,1}^E v_{ac}\sin\gamma = f(a,\gamma)$$
$$2\omega\frac{d\gamma}{dT_2} = 2\omega\sigma - \frac{Sa^2}{\omega} + \frac{k_{0,1}^E v_{ac}}{a}\cos(\gamma) = g(a,\gamma) \quad (50)$$

By setting $\frac{da}{dT_2}$ and $\frac{d\gamma}{dT_2}$ zero in Eq. (50), the governing equation of the equilibrium points (a_0, γ_0) can be written as follows

$$a_0^2\left[\left(\frac{k_l^v}{k_l^I}\omega\right)^2 + \left(\frac{Sa_0^2}{\omega} - 2\omega\sigma\right)^2\right] = \left(k_{0,1}^E v_{ac}\right)^2 \quad (51)$$

According to Eq. (51), the maximum amplitude (a_0) is reached when the expression inside the second parenthesis equals to zero.

$$a_0 = \frac{k_{0,1}^E k_l^I v_{ac}}{k_l^v \omega} \quad , \quad \sigma = \frac{Sa_0^2}{2\omega^2} \quad (52)$$

The nonlinear resonance frequency is obtained by inserting $\Omega = \omega + \varepsilon^2\sigma$ in Eq. (52), as follows

$$\Omega = \omega + \frac{S\left(k_{0,1}^E k_l^I v_{ac}\right)^2}{2\left(k_l^v \omega^2\right)^2} \quad (53)$$

6. Stability and instability analysis

Stable stationary resolution is obtained by means of Jacobian matrix, which can be calculated by employing Eq. (50).

$$\begin{bmatrix}\Delta a' \\ \Delta\gamma'\end{bmatrix} = \frac{1}{\bar{m}}\begin{bmatrix}\frac{\partial f}{\partial a} & \frac{\partial f}{\partial \gamma} \\ \frac{\partial g}{\partial a} & \frac{\partial g}{\partial \gamma}\end{bmatrix}\begin{bmatrix}\Delta a \\ \Delta\gamma\end{bmatrix} = \frac{1}{2\omega}\times$$
$$\begin{bmatrix} -\frac{k_l^v}{k_l^I}\omega & k_{0,1}^E v_{ac}\cos\gamma_0 \\ \frac{-2Sa_0}{\omega} - \frac{k_{0,1}^E v_{ac}\cos\gamma_0}{a_0^2} & \frac{-k_{0,1}^E v_{ac}}{a_0}\sin\gamma_0\end{bmatrix}\begin{bmatrix}\Delta a \\ \Delta\gamma\end{bmatrix} \quad (54)$$

Let us perceive coefficient matrix as B, then the characteristic matrix of the system can be calculated when the determinant of the matrix (B−λI) is equal to zero. It should be noted that I is the unit matrix and λ is the characteristic equation root. By substituting the achieved equation into Eq. (50) the following result is gained.

$$\lambda^2 + \frac{2k_l^v\omega}{k_l^I}\lambda + \left[\frac{\left(k_l^v\omega\right)^2}{\left(k_l^I\right)^2} + \left(2\omega\sigma - \frac{3Sa_0^2}{\omega}\right)\left(2\omega\sigma - \frac{Sa_0^2}{\omega}\right)\right] = 0 \quad (55)$$

Hence, the characteristic equation root can be demonstrated as

$$\lambda_{1,2} = -\frac{k_l^v\omega}{k_l^I} \pm \sqrt{-\left(2\omega\sigma - \frac{3Sa_0^2}{\omega}\right)\left(2\omega\sigma - \frac{Sa_0^2}{\omega}\right)} \quad (56)$$

The instability happens when each of the eigenvalues is positive and when one of the mentioned eigenvalues becomes zero the bifurcation point occurs.

Eq. (55) results in

$$\left[\frac{\left(k_l^v\omega\right)^2}{\left(k_l^I\right)^2} + \left(2\omega\sigma - \frac{3Sa_0^2}{\omega}\right)\left(2\omega\sigma - \frac{Sa_0^2}{\omega}\right)\right] = 0 \quad (57)$$

7. Results and discussion

The succeeding results have been obtained for a micro resonator (Nayfeh and Pai) with the geometrical and mechanical properties according to Table 1. It should be noted that the other parameters of the system are stated in the legends and captions of figures.

Table 1 Geometrical and mechanical properties of the considered configuration

l_b	w_b	t_b	E_b	ρ_b
510 μm	100 μm	1.5 μm	169 GPa	$2330\frac{\text{kg}}{\text{m}^3}$
D	ε_0	ρ_v	w_v	E_v
1.18 μm	8.854e-12	$2230\frac{\text{kg}}{\text{m}^3}$	100 μm	105G9 Pa

Considering Eqs. (51)-(53), the nonlinear vibration amplitude and nonlinear shift of resonance frequency are primarily influenced by electrostatic excitation, bending curvature, inertia, natural frequency, electrostatic force, and viscoelastic damping. It is worth reminding that softening effect arises from nonlinear electrostatic excitation and nonlinear inertia while the hardening effect is due to the nonlinear bending curvature.

It demonstrates that the nonlinear behavior of the system, under the electrostatic excitation, follows hardening phenomenon when $F \neq 0$ and $S > 0$, which means $\frac{\Omega}{\omega} > 1$. On the contrary, when $F \neq 0$ and $S < 0$, the nonlinear behavior of the system denotes a softening phenomenon, which means $\frac{\Omega}{\omega} < 1$. The variations of nonlinear coefficients, S with respect to the variations of DC electrostatic voltage is presented in Fig. 3.

As is seen in Fig. 3, as $\alpha_3 V_{dc}^2$ increases the value of S starts from zero and tends to the large negative values. This decrease is the result of variation in the sum of the $K_{q,0}^E, K_{c,0}^E, K_q^G, K_c^G, K_q^I$ and K_c^I coefficients. Fig. 3

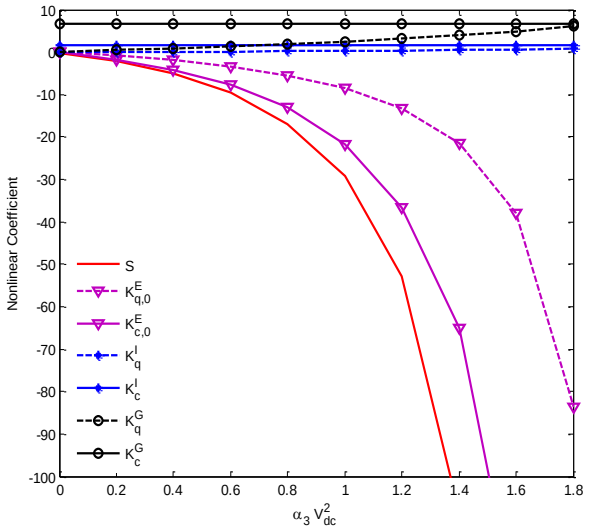

Fig. 3 Nonlinear coefficient alteration with respect to $\alpha_3 V_{dc}^2$ where $\alpha_1 = 0.2$,l_v=0.5l_b, t_v=0.5 μm

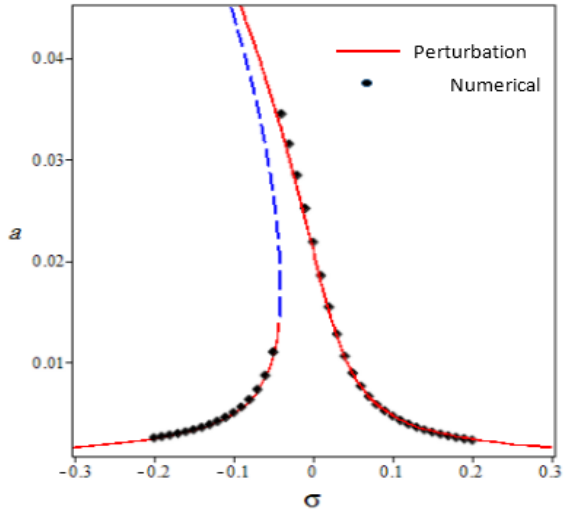

Fig. 4 Runge-Kutta method and multiple scale perturbation theory comparison where l_1=0.25l_b, l_2=0.75l_b, α_2=0.015, $\alpha_3 V_{dc}^2$=1.5, v_{ac}=0.0003

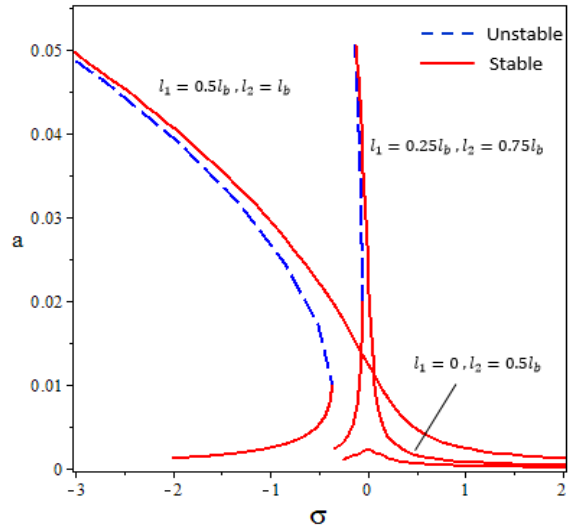

Fig. 5 Viscoelastic layer resonance shift diagram in three different locations l_1=0.5l_b, t_v=0.5 μm, C=260000 Pa.s, v_{ac}=0.0005

indicates that the rise in the value of $\alpha_3 V_{dc}^2$ results in the decrease of the second and third-order nonlinear coefficients ($K_{q,0}^E, K_{c,0}^E$), which are the softening factors and arisen from the second and third-order terms of electrostatics excitation, from zero to negative values with a rapid rate. The value of K_q^G, which is a hardening factor and due to the second-order geometrical nonlinear terms, changes from zero to the positive quantities with a slow rate. K_c^G , which is a hardening factor and due to the third-order geometrical nonlinear terms, indicates a positive value and it slightly alters by increase of $\alpha_3 V_{dc}^2$. Regarding K_q^I and K_c^I, which fit into the softening factors arising from second and third-order inertial terms, both value and trend are moderate. It can be implied from Fig. 3 that hardening terms are dominant for very low electrostatic voltage. However, a slight increase in the electrostatic voltage makes $K_{q,0}^E$ and $K_{c,0}^E$ terms dominant. It means that by an increase on the value of electrostatic actuation the softening behavior increases. This obtained outcome verifies the results of previous works by Nayfeh *et al.* (2007), Younis and Nayfeh (2003) and Chaterjee and Pohit (2009), in which the effect of electrostatic actuation was considered. The results of this paper can be verified quantitatively by comparing analytical perturbation solution and numerical solution. The numerical solution is obtained using Maple17 software based on Runge Kutta Fehlberg Method algorithm. This algorithm which is called RKF45 finds a numerical solution using both of fifth and fourth order Runge Kutta. For solving the equation, first of all, the initial condition is considered equal to zero, and the excitation frequency is considered less than the obtained frequency from the perturbation solution for maximum amplitude. Then the amplitude of the steady state solution is called from the time history of numerical solution. Afterwards the excitation frequency is a little bit increased and the steady state of previous step is considered as the initial condition of the next step. In all of the steps the velocity initial condition is considered equal to zero. Fig. 4 proves the effectiveness of the perturbation theory for solving the problem.

Now the effect of viscoelastic layer position is studied on the frequency response function of system where the viscoelastic layer is deposited on the half of micro beam length. As observed in Fig. 5, as the viscoelastic patch gets closer to the free end of the micro beam, the nonlinear resonance shifts and also the steady state amplitude at resonance frequency increases. It shows that the optimum case occurs when the viscoelastic layer is deposited on the middle part of micro beam length since it has enough amplitude and has no effective nonlinear shift of resonance frequency. It is observed that when one end of viscoelastic layer is at the free side of micro beam a large nonlinear shift of resonance frequency, which is undesirable for sensor application, is presented. It must be noted that if the amount of viscoelastic damping decreases then considering Eq. (53)

the steady state amplitude in resonance frequency increases. So for small value of viscoelastic layer, the case that its left end of viscoelastic layer is constrained at the clamped side would be the desirable configuration.

The demonstrated behavior in Fig. 5 can be explained by Eqs. (49)-(52). It can be claimed from the mentioned equations that the stable amplitude is directly proportional to excitation force coefficients ($K_{0,1}^{E}$) and linear term due to inertia (K_l^I) and they are inversely proportional to natural frequency (ω) and linear coefficient arisen from viscoelastic damping (K_l^v). It is transparent that flexural stiffness diminishes as the second layer moves towards micro-beam from the clamp side. The decrease of flexural stiffness causes an increase in the static deformation. On the other hand, as is seen in equation appendix A, $K_{0,1}^{E}$ is due to the stimulation in the denominator containing $(W_s-1)^2$ and as a result its value rises, obeying nonlinear behavior. With respect to the linear terms of Eq. (37), $K_l^I\ddot{P}+K_l^v\dot{P}+(K_{l,1}^{E}+K_l^G)P$, natural frequency is directly proportional to linear electrostatic force ($K_{l,0}^{E}$). With regard to appendix A, for calculating $K_{l,0}^{E}$, the term $(W_s-1)^3$ is located in the denominator of the integral. Therefore, natural frequency is also decreased in a nonlinear manner by the movement of the second layer from the clamp side towards the free side of the micro-beam. The result of these variations, with respect to Eqs. (49)-(52), leads to the increase of amplitude in a resonance with the movement of viscoelastic layer from the clamp side towards the free side. It should be noted that the variations of the other terms like K_l^I and K_l^v are negligible in comparison. As is observed in Fig. 3, when electrostatic voltage is $V_{dc}>0.3$, electrostatic nonlinear coefficients are much more noticeable than inertial and geometrical nonlinear coefficients. Hence, the major nonlinear behavior should be sought in $K_{q,0}^{E}$ and $K_{c,0}^{E}$. With respect to Appendix A, the rise in the static deformation due to the viscoelastic layer movement leads to nonlinear growth of $K_{q,0}^{E}$ and $K_{c,0}^{E}$ since the terms $(W_s-1)^4$ and $(W_s-1)^5$ are situated in the denominators of these expressions. The increase of S due to the softening phenomenon slows the growth rate of $K_{0,1}^{E}$ and, on the other hand, the decrease of ω results in the shift of linear resonance with respect to the viscoelastic layer movement.

In follow, the viscoelastic layer volume is assumed as constant and its length and thickness are simultaneously changed in order to obtain the optimized thickness, length, and position. The value of the volume is considered equal to $12750\mu m$ which is equivalent to a layer with thickness of $t_v=0.25\mu m$ deposited on the entire length of micro beam. Subsequently, the viscoelastic layer length is decreased and its thickness is increased in three different cases as shown in Fig. 6. In any case, it is assumed that the viscoelastic layer is initially deposited on the entire length of micro beam. In the first case, one end of the coated layer is considered fixed at the clamped side of the micro cantilever, and then its length is decreased from the other side, where its thickness is increased (Fig. 6(a)). In the second case, one end of the coated layer is constrained at the free side of micro cantilever, and then its length is decreased from the other side, where its thickness is increased (Fig. 6(b)). In the third case, the length of viscoelastic layer is decreased from both left and right ends, where its thickness is expanded (Fig. 6(c)).

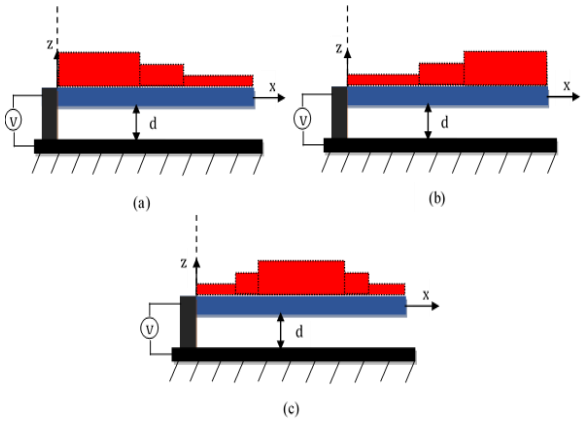

Fig. 6 The viscoelastic layer with a constant volume in three different cases

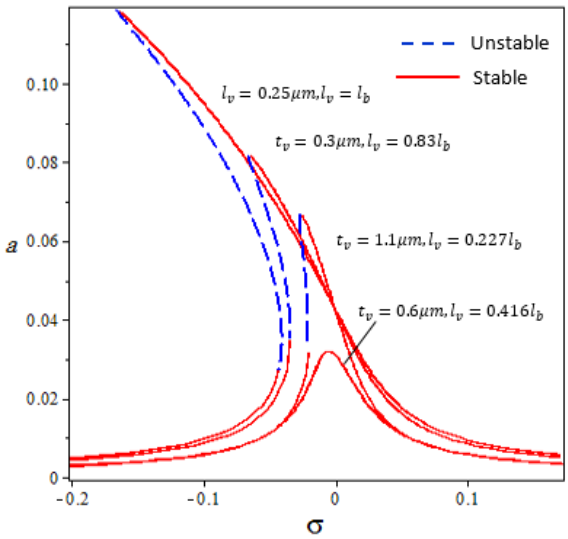

Fig. 7 The steady state amplitude alterations with respect to σ for different viscoelastic layer thicknesses in the first case where $C=32000Pa.s$, and $v_{ac}=0.001$

Since the volume is considered as constant in this section, the length of the viscoelastic layer is merely specified in the following figures.

Fig. 7 indicates that by simultaneous change of thickness and length of viscoelastic layer according to the case (a) of Fig. 6 from $t_v=0.25\mu$m and $l_v=l_b$ to a specific value, here, $t_v=0.6\mu$m and $l_v=0.416667l_b$, the nonlinear shift of resonance frequency increases and after that it shows a reverse trend. It can be observed from Fig. 7 that the steady state amplitude at resonance frequency has a downward trend within a specific range and it then shows an upward trend.

As shown in Fig. 7, the most optimum state of a resonator sensor can be seen when the viscoelastic layer is deposited on approximately less than half length of micro beam and more than a quarter of micro beam length for example in $t_v=0.6\,\mu$m. Under this condition, the system

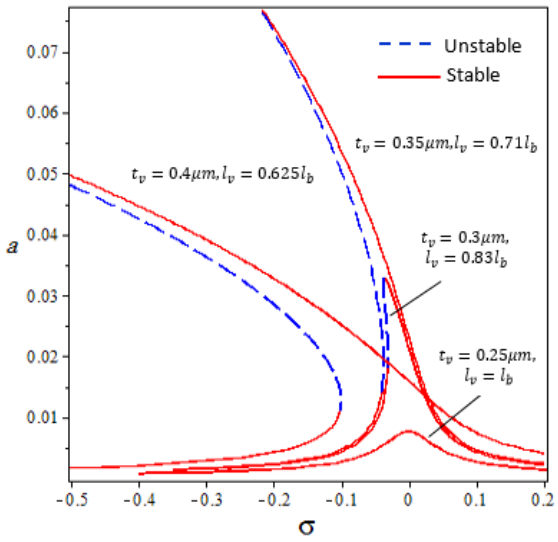

Fig. 8 The steady state amplitude alterations with respect to σ for different viscoelastic layer thicknesses in the second case where C=148000 Pa.s, and v_{ac}=0.0003

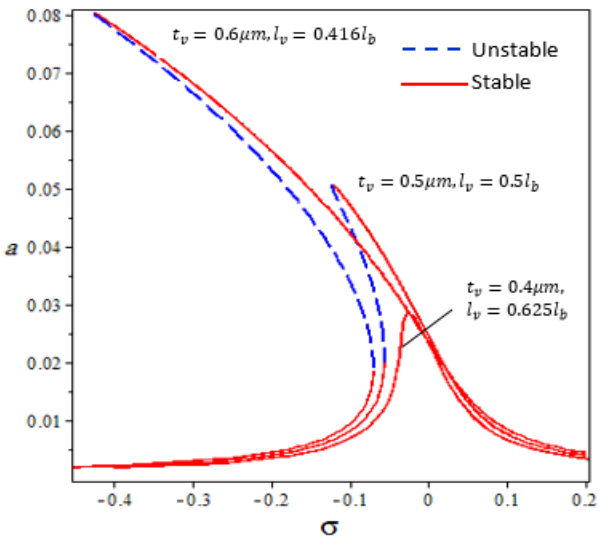

Fig. 9 The steady state amplitude alterations with respect to σ for different viscoelastic layer thicknesses in the third case where when C=260000 Pa.s, and v_{ac}=0.0005

follows a small nonlinear shift of resonance frequency, the viscoelastic layer covers enough length of the micro beam, and the steady state amplitude at resonance frequency is large enough.

Fig. 8 represents that by simultaneous change of thickness and length of viscoelastic layer according to case (b) of Fig. 6, the nonlinear shift of resonance frequency and also steady state amplitude at resonance frequency increase. It demonstrates that the optimum state is when the viscoelastic layer is deposited on approximately more than 0.75 of the micro beam length. The coated length less than this value causes a large nonlinear shift of resonance frequency.

Fig. 9 gives an indication of the frequency response function by simultaneous change of thickness and length of viscoelastic layer according to case (c) of Fig. 6. It demonstrates that the optimum state is when the viscoelastic layer is deposited on approximately more than half of the micro beam length.

Comparing Figs. 7, 8 and 9 demonstrate that if the value of viscoelastic damping is small enough in order to have a steady state amplitude at resonance frequency which is large enough, then the best configuration is the case that viscoelastic layer is deposited from fixed side to the middle part of micro beam. It is observed that the best configuration for large value of viscoelastic damping is depositing viscoelastic layer on the middle part of micro beam with a length approximately equal to the half-length of micro beam.

As is presented in Fig. 6, in case (a), as the length of the viscoelastic layer decreases, firstly, flexural stiffness increases, because of thickness growth in the clamp side, then when the length decrease reaches a specific amount, flexural stiffness decreases since the micro beam behaves like a single layer beam which is located in the end of the second layer. In case (b), flexural stiffness has a decreasing rate owing to the length decline in the clamp side of the micro-beam. Case (c) is almost similar to case (b) but its variation rate is slower since the thickness of the free side declines and the thickness of the middle part, which has more deflection than the end part, grows. Flexural stiffness alteration leads to the static deformation as well as the frequency response change.

8. Conclusions

The vibration of an electrostatically excited micro cantilever beam is studied in this work. The micro cantilever beam is patched by a viscoelastic layer and the inertia, curvature, and electrostatic actuation nonlinearities are taken into consideration. The nonlinear motion equation is extracted by means of Hamilton principle, considering nonlinear shortening effect for Euler-Bernoulli beam. The viscoelastic model is considered as Kelvin-Voigt. In order to discretize the governing equation of motion, the Galerkin method is used with the employment of non-uniform micro cantilever beam linear free vibration mode shapes as comparison function. The multiple scale perturbation approach is applied for solving the equation of motion. The solution is verified by comparing perturbation analytical solution with Runge-Kutta numerical solution. The acquired results prove that the nonlinear vibration amplitude and resonance shift are primarily influenced by electrostatic excitation, nonlinear curvature, inertia, natural frequency, electrostatic force, and viscoelastic damping, where It is worth reminding that softening effect arises from electrostatic excitation and nonlinear inertia while the hardening effect is due to the nonlinear bending curvature. It is observed that stable amplitude declines as a result of the viscoelastic movement from the free side towards the clamp side of the micro-beam and nonlinear frequency gets closer to the natural frequency which means the softening behavior of the system decreases. Afterwards a viscoelastic layer, which covers the whole micro-beam length, is taken into account. It is seen that, by the assumption of constant

volume, as the length of this layer reduces towards the clamp side, initially the system softening reduces and after a specific length it goes up. It should be noted that as the length of this layer reduces towards the free side, the system softening increases. Another point which needs to be highlighted is that the decrease of the viscoelastic layer length towards the middle of the micro-beam, the softening phenomenon grows with a lower rate in comparison with the mentioned state.

It has been observed that when the coefficient of viscoelastic damping is small, then the best configuration for microsenser based on the shift of resonance frequency is the case that viscoelastic layer is deposited from fixed side to the middle part of micro beam. It is observed that when the coefficient of viscoelastic damping is larger, then the best configuration is depositing viscoelastic layer on the middle part of micro beam with a length approximately equal to the half-length of micro beam. It demonstrates that the worst condition is when it is deposited with an end at the free side and a length smaller than half length of micro beam.

References

Abdel-Rahman, E.M., Younis, M.I. and Nayfeh, A.H. (2002), "Characterization of the mechanical behavior of an electrically actuated microbeam", *Micromech. Microeng.*, **12**(6), 759-766.

Aboelkassem, Y., Nayfeh, A.H. and Ghommem, M. (2010), "Biomass sensor using an electrostatically actuated microcantilever in a vacuum microchannel", *Microsyst. Technol.*, **16**(10), 1749-1755.

Bataineh, A.M. and Younis, M.I. 2015, "Dynamics of a clamped-clamped microbeam resonator considering fabrication imperfections", *Microsyst. Technol.*, **21**(11), 2425-2434.

Beeby, S., Ensell, G., Kraft, M. and White, N. (2004), *MEMS Mechanical Sensors*, Artech House, Inc, Boston, London.

Boudjiet, M.T., Bertrand, J., Mathieu, F., Nicu, L., Mazenq, L., Leïchlé, T., Heinrich, S. M., Pellet, C. and Dufour, I. (2015), "Geometry optimization of uncoated silicon microcantilever-based gas density sensors", *Sens. Actuat. B: Chem.*, **208**, 600-607

Chaterjee, S. and Pohit, G.A. (2009), "Large deflection model for the pull-in analysis of electrostatically actuated microcantilever beams", *J. Sound Vib.*, **322**(4-5), 969-986.

Chitsaz Yazdi, F. and Jalali, A. (2015), "Vibration behavior of a viscoelastic composite microbeam under simultaneous electrostatic and piezoelectric actuation", *Mech. Time-Depend. Mater.*, **19**(3), 277-304.

Dufour, I., Lochon, F., Heinrich, S.M., Josse, F. and Rebiere, D. (2007), "Effect of coating viscoelasticity on quality factor and limit of detection of microcantilever chemical sensors", *Sens. J.*, **7**(2), 230-236.

Fu, Y.M., Zhang, J. and Bi, R.G. (2009), "Analysis of the nonlinear dynamic stability for an electrically actuated viscoelastic microbeam", *Microsyst. Technol.*, **15**(5), 763-769.

Ghayesh, M.H., Farokhi, H. and Alici, G. (2015), "Size-dependent electro-elasto-mechanics of MEMS with initially curved deformable electrodes", *Int. J. Mech. Sci.*, **103**, 247-264.

Hoseini, S.M., Shooshtari, A., Kalhori, H. and Mahmoodi, S.M. (2014), "Nonlinear-forced vibrations of piezoelectrically actuated viscoelastic cantilevers", *Nonlin. Dyn.*, **78**(1), 571-583.

Huang, Y.T., Chen, H.L. and Hsu, W. (2014), "An analytical model for calculating the pull-in voltage of micro cantilever beams subjected to tilted and curled effects", *Microelec. Eng.*, **125**, 73-77.

Kim, I.K. and Lee, S.I. (2015), "Nonlinear resonances of a single-wall carbon nanotube cantilever", *Physica E: Low-dimens. Syst. Nanostruct.*, **67**, 159-167.

Lizhoung, X. and Xiaoli, J. (2007), "Electromechanical coupled nonlinear dynamics for microbeams", *Arch. Appl. Mech.*, **77**(7), 485-502.

Mahmoodi, S.N., Afshari, M. and Jalili, N. (2008), "Nonlinear vibrations of piezoelectric microcantilevers for biologically-induced surface stress sensing", *Commun. Nonlin. Sci. Numer. Simul.*, **13**(9), 1964-1977.

Mahmoodi, S.N., Khadem, S.E. and Kokabi, M. (2007), "Non-linear free vibrations of Kelvin-Voigt visco-elastic beams", *Int. J. Mech. Sci.*, **49**(6), 722-732.

Masri, K.M. and Younis, M.I. (2015), "Investigation of the dynamics of a clamped-clamped microbeam near symmetric higher order modes using partial electrodes", *Int. J. Dyn. Control*, **3**(2), 173-182.

Najar, F., El-Borgi, S., Reddy, J.N. and Mrabet, K. (2015), "Nonlinear nonlocal analysis of electrostatic nanoactuators", *Compos. Struct.*, **120**, 117-128.

Nayfeh, A.H. and Pai, P.F. (2004), *Linear and Nonlinear Structural Mechanics*, Wiley, New York.

Nayfeh, A.H. and Younis, M.I. (2005), "Dynamics of MEMS resonators under superharmonic and subharmonic excitations", *Micromech. Microeng.*, **15**(10), 1840-1847.

Nayfeh, A.H., Younis, M.I. and Abdel-Rahman, E.M. (2007), "*Dynamic pull-in phenomenon in MEMS resonators*", *Nonlin. Dyn.*, **48**(1), 153-163.

Nie, M., Huang, Q. and Li, W. (2006), "Measurement of material properties of individual layers for composite films by a pull-in method", *J. Phys. Conf. Ser.*, **34**(34), 516-521.

Poloei, E., Zamanian, M. and Hosseini, S.A.A. (2015), "Static deflection and natural frequency analysis of two-layered electrostatically actuated microcantilever for finding the optimum configuration", *Mod. Mech. Eng.*, **15**(5), 245-253.

Raeisifard, H., Zamanian, M., Nikkhah Bahrami, M., Yousefi-Koma, A. and Raeisi Fard, H. (2014), "On the nonlinear primary resonances of a piezoelectric laminated micro system under electrostatic control voltage", *J. Sound Vib.*, **333**(21), 5494-5510.

Rahaeifard, M. and Ahmadian, M.T. (2015), "On pull-in instabilities of microcantilevers", *Int. J. Eng. Sci.*, **87**, 23-31.

Rasekh, M. and Khadem, S.E. (2011), "Pull-in analysis of an electrostatically actuated nano-cantilever beam with nonlinearity in curvature and inertia", *Int. J. Mech. Sci.*, **53**(2), 108-115.

Rasekh, M. and Khadem, S.E. (2013), "Design and performance analysis of a nanogyroscope based on electrostatic actuation and capacitive sensing", *J. Sound Vib.*, **332**(23), 6155-6168.

Rezazadeh, G. (2008), "A comprehensive model to study nonlinear behavior of multilayered micro beam switches", *Microsyst. Technol.*, **14**(1), 135-141.

Rezazadeh, G., Keyvani, A. and Jafarmadar, S. (2012), "On a MEMS based dynamic remote temperature sensor using transverse vibration of a bi-layer micro-cantilever", *Measur.*, **45**(3), 580-589.

Shooshtari, A., Hoseini, S.M., Mahmoodi, S.N. and Kalhori, H. (2012), "Analytical solution for nonlinear free vibrations of viscoelastic microcantilevers covered with a piezoelectric layer", *Smart Mater. Struct.*, **21**(7), 75015- 75025.

Sun, W., Sun, Y., Yu, Y. and Zheng, S. (2016), "Nonlinear vibration analysis of a type of tapered cantilever beams by using an analytical approximate method", *Struct. Eng. Mech.*, **59**(1), 1-14.

Wang, K.F. and Wang, B.L. (2015), "A general model for nano-

cantilever switches with consideration of surface effects and nonlinear curvature", *Physica E: Low-dimens. Syst. Nanostruct.*, **66**, 197-208.

Yang, W.D. and Wang, X. (2016), "Nonlinear pull-in instability of carbon nanotubes reinforced nano-actuator with thermally corrected Casimir force and surface effect", *Int. J. Mech. Sci.*, **107**, 34-42.

Younis, M. I. (2011), *MEMS Linear and Nonlinear Statics and Dynamics*, Springer US, New York.

Younis, M.I. (2015), "Multi-mode excitation of a clamped-clamped microbeam resonator", *Nonlin. Dyn.*, **80**(3), 1531-1541.

Younis, M.I. and Alsaleem, F. (2009), "Exploration of new concepts for mass detection in electrostatically-actuated structures based on nonlinear phenomena", *J. Comput. Nonlin. Dyn.*, **4**(2), 021010-021025.

Younis, M.I. and Nayfeh, A.H. (2003), "A Study of the nonlinear response of a resonant microbeam to an electric actuation", *Nonlin. Dyn.*, **3**(1), 91-117.

Zamanian, M. and Karimiyan, A. (2015), "Analysis of the mechanical behavior of a doubled microbeam configuration under electrostatic actuation", *Int. J. Mech. Sci.*, **93**, 82-92.

Zamanian, M. and Khadem, S.E. (2010), "Nonlinear vibration of an electrically actuated microresonator tuned by combined DC piezoelectric and electric", *Smart Mater. Struct.*, **19**(1), 15012-15031.

Zamanian, M., Khadem, S.E. and Mahmoodi, S.N. (2010), "Nonlinear response of a resonant viscoelastic microbeam under an electrical actuation", *Struct. Eng. Mech.*, **35**(4), 387-407.

CC

Appendix A

$$K_{0,1}^{E}=-2\alpha_3 V_{dc}\int_0^1\frac{\Phi(x)}{(w_s(x)-1)^2}dx$$

$$K_{0,2}^{E}=-\alpha_3\int_0^1\frac{\Phi(x)}{(w_s(x)-1)^2}dx$$

$$K_l^I=\int_0^1 m(x)\Phi^2(x)dx$$

$$-\alpha_1\int_0^1\left(\frac{d}{dx}\Phi(x)\right)\left(\frac{d}{dx}w_s(x)\right)\times$$

$$\int_1^x m(x)\int_0^x\left(\frac{d}{dx}\Phi(x)\right)\frac{d}{dx}w_s(x)dxdxdx$$

$$K_{l,0}^{E}=2\alpha_3 V_{dc}^{\ 2}\int_0^1\frac{\Phi^2(x)}{(w_s(x)-1)^3}dx$$

$$K_{l,1}^{E}=2\alpha_3 V_{dc}\int_0^1\frac{\Phi^2(x)}{(w_s(x)-1)^3}dx$$

$$K_{l,2}^{E}=2\alpha_3\int_0^1\frac{\Phi^2(x)}{(w_s(x)-1)^3}dx$$

$$K_l^G=\int_0^1 H_1(x)\left(\frac{d^2}{dx^2}\Phi(x)\right)^2dx+$$

$$4\alpha_1\left(\int_0^1 H_1(x)\left(\frac{d^2}{dx^2}\Phi(x)\right)\left(\frac{d}{dx}\Phi(x)\right)\times\right.$$

$$\left.\left(\frac{d}{dx}w_s(x)\right)\left(\frac{d^2}{dx^2}w_s(x)\right)dx\right)+$$

$$\alpha_1\left(\int_0^1 H_1(x)\left(\frac{d^2}{dx^2}\Phi(x)\right)^2\left(\frac{d}{dx}w_s(x)\right)^2dx\right)+$$

$$\alpha_1\left(\int_0^1 H_1(x)\left(\frac{d}{dx}\Phi(x)\right)^2\left(\frac{d^2}{dx^2}w_s(x)\right)^2dx\right)$$

$$K_q^G=3\alpha_1\left(\int_0^1 H_1(x)\left(\frac{d^2}{dx^2}\Phi(x)\right)^2\left(\frac{d}{dx}\Phi(x)\right)\times\right.$$

$$\left.\left(\frac{d}{dx}w_s(x)\right)dx\right)+$$

$$3\alpha_1\left(\int_0^1 H_1(x)\left(\frac{d^2}{dx^2}\Phi(x)\right)\left(\frac{d}{dx}\Phi(x)\right)^2\left(\frac{d^2}{dx^2}w_s(x)\right)dx\right)$$

$$K_{q,0}^{E}=-3\alpha_3 V_{dc}^{\ 2}\int_0^1\frac{\Phi_n(x)(\Phi_m(x))^2}{(w_s(x)-1)^4}dx$$

$$K_{q,1}^{E}=-3\alpha_3 V_{dc}\int_0^1\frac{\Phi_n(x)(\Phi_m(x))^2}{(w_s(x)-1)^4}dx$$

$$K_{q,2}^{E}=-3\alpha_3\int_0^1\frac{\Phi_n(x)(\Phi_m(x))^2}{(w_s(x)-1)^4}dx$$

$$K_c^G = 2\alpha_1\left(\int_0^1 H_1(x)\left(\frac{d^2}{dx^2}\Phi(x)\right)^2\left(\frac{d}{dx}\Phi(x)\right)^2 dx\right)$$

$$K_{c,0}^E = 4\alpha_3 V_{dc}{}^2\int_0^1 \frac{\left(\Phi(x)\right)^4}{\left(w_s(x)-1\right)^5}dx$$

$$K_{c,1}^E = 4\alpha_3 V_{dc}\int_0^1 \frac{\left(\Phi(x)\right)^4}{\left(w_s(x)-1\right)^5}dx$$

$$K_{c,2}^E = 4\alpha_3\int_0^1 \frac{\left(\Phi(x)\right)^4}{\left(w_s(x)-1\right)^5}dx$$

$$K_{q1}^I = \alpha\left(\int_0^1\left(\frac{d}{dx}\Phi(x)\right)\left(\frac{d}{dx}w_s(x)\right)\times_1\right.$$
$$\left.\int_1^x m(x)\int_0^x\left(\frac{d}{dx}\Phi(x)\right)^2 dxdxdx\right)+$$
$$\alpha_1\left(\int_0^1\left(\frac{d}{dx}\Phi(x)\right)\left(\frac{d}{dx}\Phi(x)\right)\times\right.$$
$$\left.\int_1^x m(x)\int_0^x\left(\frac{d}{dx}\Phi(x)\right)\left(\frac{d}{dx}w_s(x)\right)dxdxdx\right)$$

$$K_c^I = \alpha_1\int_0^1\left(\frac{d}{dx}\Phi(x)\right)^2\int_1^x m(x)\int_0^x\left(\frac{d}{dx}\Phi(x)\right)^2 dxdxdx$$

$$K_{q2}^I = \alpha_1\int_0^1\left(\frac{d}{dx}\Phi(x)\right)\left(\frac{d}{dx}w_s(x)\right)\times$$
$$\int_1^x m(x)\int_0^x\left(\frac{d}{dx}\Phi(x)\right)^2 dxdxdx$$

$$K_l^v = \alpha_2\int_0^1 H_2(x)\left(\frac{d^2}{dx^2}\Phi(x)\right)^2 dx +$$
$$\alpha_1\alpha_2\left(\frac{1}{2}\int_0^1 H_2(x)\left(\frac{d^2}{dx^2}\Phi(x)\right)^2\left(\frac{d}{dx}w_s(x)\right)^2 dx\right)+$$

$$(\alpha_1\alpha_2)\left(\int_0^1 H_2(x)\Phi(x)\left(\frac{d^2}{dx^2}\Phi(x)\right)\times\right.$$
$$\left.\left(\frac{d}{dx}w_s(x)\right)\left(\frac{d^2}{dx^2}w_s(x)\right)dx\right)$$